Published in final edited form as:
Biochim Biophys Acta. 2012 December ; 1818(12): 3040–3047. doi:10.1016/j.bbamem.2012.07.029.

Aggregation Behavior of Ibuprofen, cholic acid and dodecylphosphocholine micelles

Priyanka Prakash[1], **Abdallah Sayyed-Ahmad**[1,#], **Yong Zhou**[1], **David E. Volk**[2], **David G. Gorenstein**[2], **Elizabeth Dial**[1], **Lenard M Lichtenberger**[1], and **Alemayehu A Gorfe**[1]

[1]Department of Integrative Biology and Pharmacology, 6431 Fannin St., Houston, Texas 77030

[2]Institute of Molecular Medicine, University of Texas Health Science Center at Houston

Abstract

Non-steroidal anti-inflammatory drugs (NSAIDs) are frequently used to treat chronic pain and inflammation. However, prolonged use of NSAIDs has been known to result in Gastrointestinal (GI) ulceration/bleeding, with a bile-mediated mechanism underlying their toxicity to the lower gut. Bile acids (BAs) and phosphatidylcholines (PCs), the major components of bile, form mixed micelles to reduce the membrane disruptive actions of monomeric BAs and simple BA micelles. NSAIDs are suspected to alter the BA/PC balance in the bile, but the molecular interactions of NSAID-BA or NSAID-BA-PC remain undetermined. In this work, we used a series of all-atom molecular dynamics simulations of cholic acid (CA), ibuprofen (IBU) and dodecylphosphocholine (DPC) mixtures to study the spontaneous aggregation of CA and IBU as well as their adsorption on a DPC micelle. We found that the size of CA-IBU mixed micelles varies with their molar ratio in a non-linear manner, and that micelles of different sizes adopt similar shapes but differ in composition and internal interactions. These observations are supported by NMR chemical shift changes, NMR ROESY crosspeaks between IBU and CA, and dynamic light scattering experiments. Smaller CA-IBU aggregates were formed in the presence of a DPC micelle due to the segregation of CA and IBU away from each other by the DPC micelle. While the larger CA-IBU aggregates arising from higher IBU concentrations might be responsible for NSAID-induced intestinal toxicity, the absence of larger CA-IBU aggregates in the presence of DPC micelles may explain the observed attenuation of NSAID toxicity by PCs.

Keywords

Molecular dynamics; mixed micelle; cluster size; NSAID; bile acid

Introduction

Ibuprofen (IBU) belongs to the family of non-steroidal anti-inflammatory drugs (NSAIDs) commonly used to treat chronic pain and inflammation [1, 2]. NSAIDs block cyclooxygenase (COX), a key enzyme in the biosynthetic pathway of anti-inflammatory

Corresponding Authors: AAG: Tel: 713-500-7538; Alemayehu.G.Abebe@uth.tmc.edu; **LML**: Tel: 713-500-6320; Lenard.M.Lichtenberger@uth.tmc.edu.
[#]Current Address: Physics Department, Birzeit University, Birzeit, West Bank.

prostaglandins. Unfortunately, chronic oral consumption of NSAIDs results in serious side-effects, including gastrointestinal (GI) ulceration and bleeding [3]. Numerous studies have shown that these side-effects, notably those affecting the lower GI tract, are independent of COX-inhibition [4–6], and that injury to the upper GI-tract can be mitigated by administering NSAIDs in complex with phosphatidylcholines (PC) [7–9]. PC-conjugated NSAIDs have been shown to significantly reduce upper-gut toxicity without loss of efficacy [10–13]. However, it remains unclear how NSAIDs cause lower-gut injury.

Recent studies suggest that bile acids (BAs) play a key role in NSAID-related lower gut injury that affects ~80% of regular NSAID users [14–17]. For instance, bile-duct ligation in rats (which halts secretion of bile into the small intestine) prevented severe injury and perforation of the distal bowel [18], and systemic administration of indomethacin (another NSAID) was found to be most injurious in species that secrete high concentrations of the drug into bile via enterohepatic circulation [19]. Moreover, cell culture studies have shown that NSAIDs exacerbate BA-induced cell injury [20–23].

Bile acids are digestive surfactants with a unique facial amphipathicity that form non-toxic mixed micelles with PCs. BA-PC aggregation is believed to protect the hydrophobic lining of the GI-epithelium from the detergent action of monomeric BA and simple BA micelles [24–27]. A number of biophysical studies have looked at the morphology, size and dynamics of BA-PC mixed micelles [28–31]. Advances in computational power and simulations have also led to a deeper understanding of the molecular interactions governing the assembly of BA-PC and other micelle-forming mixtures [32–40]. Earlier simulations of BA-PC and BA-PC-Cholesterol [41] mixtures favored the radial-shell model proposed by Ulmius *et al* [30]. Subsequent studies [42,43] found features of a disk-shaped micelle originally proposed by Carey and Small [44]. Our own previous study on pure cholic acid (CA) and CA-dodecylphosphocholine (DPC) micelles supported the radial-shell model and revealed a linear dependence of micelle size on CA concentration [45].

The present work focuses on the aggregation behavior of BA-IBU and BA-IBU-PC mixtures. Since BA-PC micelles are already present under physiological conditions, we investigated the aggregation behavior of IBU with pre-formed DPC-CA micelles. We discuss the internal structure, molecular interactions, dynamics and morphology of the resulting mixed micelles.

Methods

The aggregation behaviors of binary and ternary mixtures of a pre-formed DPC micelle, CA (the most common BA) and IBU were studied at different molar ratios (Figure 1 and Table 1). The single tail DPC was chosen instead of a regular PC because DPCs readily assemble into micelles while two tail PCs prefer to form bilayers. We used the therapeutically most relevant S-isomer of IBU [46]. During the initial setup of the binary mixture, CA and IBU were placed randomly in a cubic box of length 72Å. Both CA and IBU possess a negative net charge (Figure 1), which was neutralized by adding Na^+ ions equivalent to the total number of CA and IBU in the simulation box. To speed up the equilibration of the ions, they were distributed randomly around the carboxyl oxygen atoms of CA and IBU using a spherical shell of inner radius 3Å and thickness 5Å. The ternary mixtures contained a pre-formed micelle of 60 DPC molecules, plus CA and IBU of variable proportions (Table 1). The starting configurations for CA and IBU were built based on the CHARMM general force field (CGenFF) [47]. The initial structure for the ternary mixture was built by randomly adding IBU molecules onto the last snapshot of a previously reported simulation of CA adsorbed on a DPC micelle [45]. Each system was then energy minimized with the steepest descent method for 100,000 steps and equilibrated as described previously [45]. All

simulations were performed with the NAMD program [48] at 310K and 1atm. Temperature was kept constant by the Langevin dynamics method with a damping coefficient of $10ps^{-1}$ and pressure by the Langevin piston method using a piston period of 200fs and decay time of 100fs. All short-range vdW interactions were truncated at 12Å using a 14Å cutoff was used for non-bonded list updates. Long-range electrostatic interactions were calculated with the particle mesh Ewald (PME) method [49] using a FFT grid of $1Å^{-1}$.

Dynamic Light Scattering (DLS)

DLS, which detects the amount of light scattered by particles in a test solution, was used to measure the average size of the micelles resulting from mixing CA and IBU at different concentrations and molar ratios. An appropriate amount of CA and/or IBU was dissolved in a phosphate buffer solution (PBS) and the solution was vortexed and allowed to equilibrate over night at room temperature. The Malvern Zetasizer Nano instrument with particle size range of 0.6 to 6μm was then used to measure the size distribution of the resulting micelles.

Nuclear Magnetic Resonance (NMR) Spectroscopy

To probe intermolecular interactions between IBU and CA, we determined the one-dimensional proton and carbon chemical shifts by NMR of each chemical alone and in combination, both above and below the critical micelle concentrations (*cmc*) of CA, which is 25–30mM. We collected a 400 ms ROESY spectrum to investigate intermolecular interactions. Varian UnityPlus 800 MHz and Bruker Avance 600MHz NMR spectrometers with cold probes were used.

Results and Discussion

In each of the five simulations (Table 1) CA and IBU spontaneously formed aggregates within the simulation timescales. The majority of these aggregates were mixed micelles of CA and IBU. Both CA and IBU were also able to adsorb onto the pre-formed DPC micelle in the two simulations of DPC-CA-IBU mixtures of different proportions. Throughout this manuscript, micelle or aggregate refers to mixed micelles of CA and IBU or CA, IBU and DPC. Where applicable, we will refer to CA-only or IBU-only micelles as pure CA and pure IBU micelles, respectively.

CA-IBU Binary Mixture

The binary CA-IBU mixtures were simulated in different molar ratio with the concentration of CA being always larger than its critical micelle concentration (*cmc*) of 25–30mM (Table 1). The concentration of IBU was kept below its *cmc* of 180mM [50], except in simulation S_A where it is higher. In each case, aggregates of varying cluster sizes (CSn, see equation 1) were observed (Figure S1). Since the hydrophobic effect governs the assembly process, distances between the hydrophobic atoms of CA and IBU were used to define CA-IBU aggregates. Thus, if IBU-C11 and CA-C18 (see Figure 1) are within 10Å from each other, these two molecules were defined as belonging to the same micelle. This cutoff was derived from the pairwise radial distributions shown in Figure S2. The stability of the simulations was monitored by the time evolution of the number of CA or IBU monomers ($N_{Monomers}$), as well as the weight and number averaged aggregation numbers N_W and N_N (Figure S3). N_W and N_N, as well as principal moments of inertia I_1, I_2 and I_3, were calculated as described before [45]. The weighted probability distribution (P_n) of micelles and monomers was calculated as:

$$P_n = \frac{X}{N} \text{ where } X = \frac{\left(\sum_{F=1}^{N_F} nCSn\right)}{N_F}. \quad (1)$$

CSn is the number of CA-IBU mixed-micelles of size n (n=2, 3, 4…) or the number of CA and IBU monomers (n = 1), F is frame index, N_F is the total number of frames sampled every 10ps and N the total number of CA and IBU molecules in the system.

The number of CA and IBU monomers monotonously decreased and stabilized to a small value (e.g. ~2.5 in S_C, see Figure S3). N_W and N_N also plateaued after ~20ns in each of the three simulations (Figure S3). The initial 30ns data was therefore regarded as the equilibration phase and was not used for further analyses. The heterogeneity of the system was determined by calculating the polydispersity index $\langle N_w \rangle / \langle N_N \rangle$, where the larger the difference between the two aggregation numbers the more polydisperse the system would be. The ensemble-averaged values of N_W and N_N and the polydispersity index for the three binary simulations are shown in Figure 2A. It is clear that at lower IBU concentrations, the number of mixed micelles decreases and polydispersity increases. Note also the smaller polydispersity index in S_A where IBU is present above its *cmc* (Figure 2A inset).

Aggregate Size—The weighted probability distribution plotted in Figure 2B shows that the mixture with the highest IBU concentration (i.e. S_A) forms micelles of size 9–10, 15–16 and 18–19. Lower IBU concentrations yielded smaller micelles: 12–13 and 15 in S_B and 7–10 in S_C (Figure 2B). Thus, the population of larger micelles increases with increasing IBU concentrations; the largest micelles of 18 or 19 molecules emerged only when the concentration of IBU was greater than its *cmc* of 180mM [50]. Our previous study [45] showed an average size of 5–6 for pure CA micelles, in agreement with experiments [51, 52]. Clearly, addition of IBU leads to larger micelles. We propose that due to their larger surface area, charge and volume, these larger particles may play a role in NSAID-induced intestinal injury.

Micelle Composition—Figure 3 displays the average number of CA (n_{CA}) and IBU (n_{IBU}) molecules within the binary micelles of different sizes. The data suggests a stepwise evolution of each of the most populated micelles. Thus, based upon the CA:IBU ratio within the aggregate, the polydisperse micelles in S_A can be divided into three groups: (I) micelles with n_{CA} = 4–5 and n_{IBU} = 2–6, (II) n_{CA} = 6–7 and n_{IBU} = 4–9 and (III) n_{CA} = 8–10 and n_{IBU} = 7–9 (Figure 3A). There are similar numbers of CA and IBU molecules in each group, but the dominant micelles contain a saturating concentration of IBU for a given number of CA. When the IBU fraction is lower (cf. S_B and S_C), the proportion of CA within the micelles becomes larger. There are no highly populated micelles in either group I or III of simulation S_B (Figure 3B). However, similar to that in S_A, group I of S_B has 5–9 CA and 0–5 IBU molecules and group III has 11–15 CA and 5–7 IBU. There is a dominant micelle of size 15 in group II, along with less populated ones made up of 6–9 CA and 4–7 IBU. Similarly, in S_C (Figure 3C), group I has 4–9 CA and 1–2 IBU, while group II involves a linear increase of CA with a roughly constant number of IBU (~3).

Interestingly, the minimum number of CA molecules in every case is ~4–5, which is similar to the aggregation number of a pure CA system [45]. On the other hand, the maximum number of CA molecules in the most populated micelle of each simulation is 9. For $n_{CA} > 9$, n_{IBU} remains small (e.g., n_{IBU} = 3 in S_C). This result suggests that IBU often interacts with pre-formed CA aggregates with steric effects being the key for limiting the number of IBU that can be accommodated within a given CA aggregate. The absence of well-populated

mixed micelles with 9 or more CA suggests preference for specific micellar organization that cannot be achieved with higher number of CA molecules.

Micelle Morphology—The morphology of the predominant micelles was examined using the ratio of the principal moments of inertia I_1/I_2 and I_2/I_3, with the condition that $I_1 \leq I_2 \leq I_3$. These ratios describe the shape of micelles in the following manner: for spherical micelles, $I_1 \approx I_2 \approx I_3$ and thus $I_1/I_2 \approx I_2/I_3 \approx 1$; for disk-like micelles $I_1 \approx I_2 \ll I_3$ and so $I_1/I_2 \approx 1$ and $I_2/I_3 \approx 0$; whereas for rodlike clusters $I_1 \ll I_2 \approx I_3$ so that $I_1/I_2 \approx 0$ and $I_2/I_3 \approx 1$. Figure 4 presents the bivariate distribution of the two ratios for selected highly populated mixed micelles. Quite interestingly, the shape of the larger micelles CS19 and CS18 is similar, with $I_1/I_2 \approx 0.75$–0.8 and $I_2/I_3 \approx 0.85$ (Figure 4A&B). The smaller micelles CS10, CS15 and CS8 in S_A, S_B and S_C, respectively, exhibit a similar distribution of I_1/I_2 versus I_2/I_3, but they are more dynamic than CS19 and CS18 (Figure 4D–F). CS10 exists in both S_A and S_C but it is more dynamic in the latter (data not shown). This difference in dynamics could be related to the compositional differences, since CS10 is made up of 3 CA and 7 IBU in S_A and 9 CA and 1 IBU in S_C. Similarly, CS15 in S_A and S_B differ in dynamics and have a CA:IBU ratio of 5:10 and 8:7, respectively (Figure 4C&E). Although we cannot rule out the possibility that a longer simulation time might further stabilize some of these micelles, there is a clear relationship between micelle stability and composition. Overall, the majority of the highly populated mixed micelles adopt a similar shape irrespective of cluster size, but their stability varies with the proportion of their constituents and therefore the internal interactions.

Molecular Packing—Inspection of the aggregation process during the simulations suggests that multiple pathways can lead to the formation of a stable mixed micelle (Figure 5). The most important mechanisms include: (A) the simultaneous assembly of CA and IBU, (B) formation of CA micelles followed by adsorption of IBU, and (C) merging of pre-formed CA and IBU micelles. While each mechanism can independently lead to larger micelles, the preferred mechanism appears to involve multiple steps (Figure 5). Typically, smaller aggregates are formed first via mechanism A followed by fusion via the other two mechanisms. In terms of reactant concentration, our data can be categorized into cases where both CA and IBU are above their respective *cmc* and when IBU exists below its *cmc*. In both cases, some clusters evolve via mechanism A, but in the latter monomeric IBUs can also interact with pre-formed CA micelles (mech B). However, for cases where both [IBU] and [CA] > *cmc*, the preferred mechanism of assembly is fusion of preformed CA and IBU micelles (mech. C). In few instances, IBU clusters also interact with monomeric CA (not shown).

Irrespective of the aggregation mechanism, however, once formed, mixed micelles undergo internal re-organization to achieve a specific packing arrangement between CA and IBU (Figure 5). This is most prominent for the larger micelles CS19, CS18 and CS15. The re-organization involves the insertion of the hydrophobic tail of IBU into the core of the micelle to participate in interactions with the hydrophobic β-face of CA. Both the hydrophilic face of CA and the head of IBU point toward the aqueous medium (Figure 6A).

This observation is supported by distance distributions of selected hydrophobic and hydrophilic (oxygen) atoms of CA and IBU (Figure 6B). IBU-C12 and CA-C18 lie at ~4–5Å and 7–9Å away from the center of the micelle while oxygen atoms of CA and IBU are at ~11–13Å and ~14–16Å, respectively. This indicates that the packing of the hydrophobic portions represents the most important intermolecular interaction between IBU and CA. IBU is relatively more buried than CA to allow for strong β-face-to-tail CA-IBU packing. Thus, the facially amphipathic CA molecules form a ring around the perimeter of the semi-spherical micelle while the head-tail amphipathic IBU inserts deep into the core. This

requirement for a specific packing arrangement between CA and IBU introduces an entropic penalty that limits the size of the micelle, as is typical for nonionic detergents. The similar packing arrangement among micelles of different sizes also explains their morphological similarity.

Experimental Verification—The intermolecular interactions in CA:IBU mixed micelles were examined using NMR chemical shifts and 2D ROESY spectra. Above CA *cmc*, but not below it, proton chemical shift changes (Figure 7A) were observed for both CA and IBU when mixed 1:1 at 25mM, indicating a possible interaction between the two molecules above the CA *cmc*. This was verified by ROESY cross peaks (Figure 7B, Table 2) showing detailed atomic interactions between the IBU tail and the hydrophobic face of CA (Figure 7B). This β-face-to-tail packing in the mixed micelles is in perfect agreement with the simulation results.

DLS further confirmed the ability of CA to form aggregates at concentrations above its *cmc*; no IBU aggregation was observed at a similar concentration. The binary mixture of CA and IBU below CA's *cmc* also exhibited no potential to form aggregates. However, mixing CA (above *cmc*) and IBU shows an increase in the number of aggregates (Figure 7C). Moreover, the size of the micelle(s) increases non-linearly upon increasing IBU concentrations until a plateau is reached at about a 1:3 CA:IBU ratio (Figure 7C inset). This is consistent with the non-linear dependence of the size distribution of CA-IBU micelles observed in the simulations.

DPC-CA-IBU Ternary Mixture

We investigated the aggregation behavior of IBU with a pre-formed DPC-CA micelle to gain insights into how NSAIDs might perturb naturally occurring BA-PC micelles. Following our previous analysis of CA adsorption on a DPC micelle [45], IBU binding was defined based upon a distance criterion that if C8 and C9 of IBU are within 6Å from the surface of the DPC micelle, the IBU molecule is considered bound. The number of adsorbed IBU molecules (N_{ads}) and other parameters such as radius of gyration (R_g) and solvent accessible surface area (SASA) were monitored to gauge the stability and equilibration of the system. Figure S4 shows that these parameters equilibrated within the first ~30ns of each simulation. Thus, as in the binary mixtures, the first 30ns was considered an equilibration phase of micellization and excluded from further analyses.

Aggregation Behavior of CA-IBU in the presence of DPC—The aggregation behavior of CA and IBU in the presence of a DPC micelle was evaluated based on ensemble averaged N_W and N_N, which were defined in the same way as in our analysis of the binary CA-IBU mixtures. Compared to the data from simulation S_A (i.e., the 1:1 CA:IBU binary mixture in the absence of DPC), both N_W and N_N were reduced by half in S_D (14.1 ± 0.7 & 12.7 ± 0.7 in S_A versus 7.7 ± 0.7 & 6.0 ± 0.5 in S_D). This could be due to the lower concentration of both CA and IBU in S_D. However, this does not hold for S_E where N_W and N_N are 6.5 ± 0.6 & 4.4 ± 0.8, which are not very different from those in S_D despite the concentrations of CA and IBU being significantly lower in S_E. Although not conclusive, this result suggests that the DPC micelle modulates the size of CA:IBU micelles, a notion also supported by the similar size distributions of CA:IBU micelles in both S_D and S_E (Figure 8A). Interestingly, fewer and smaller CA-IBU clusters were observed on the surface of the DPC micelle (Figure 8A). This shows that the DPC micelle affects the aggregation behavior of CA and IBU, favoring smaller micelles. To further investigate this issue, we calculated the average distance between (i) CA and IBU pairs within the dominant CA:IBU micelle in the aqueous phase (CS10) and (ii) those on the surface of the DPC micelle (CS3, CS5 etc.).

The result is shown in Figure 8B. Clearly, the DPC micelle segregated CA and IBU onto opposite poles and thereby reduced their potential to form larger mixed micelles.

Orientation of IBU and CA on a DPC-CA micelle—The internal structure of the DPC-CA-IBU ternary micelle was examined using the 2D radial distribution, Ω(r), of selected atoms of each molecule, calculated as described earlier [45] (Figure 9A). The orientation and radial distribution of CA around the DPC micelle is the same as that reported for a DPC-CA binary mixture [45]. The methyls on the hydrophobic tail of IBU penetrate into the DPC micelle, lying near the C6 carbon atom of DPC. In fact, the insertion depths of the IBU hydrophobic tail atoms C11/C12 and CA hydrophobic face atoms C18/C19 are identical and equal to about half of the DPC micelle's hydrophobic thickness. Thus, the hydrophobic regions of both IBU and CA penetrate the micelle halfway to the center. In contrast, the carboxyl oxygen atoms of both CA and IBU (see CA-O1 and IBU-O1 in Figure 9A) populate the region 18–25Å away from the micelle center, coinciding with the location of the phosphate groups of DPC.

To further analyze the organization of IBU in the ternary micelle, we used two order parameters: ϕ_1 and ϕ_2. ϕ_1 was defined as an angle between vectors $M_{center} \rightarrow$ C10 and C10 $\rightarrow$ C11 (representing the hydrophobic region of IBU) and ϕ_2 as the angle between vectors $M_{center} \rightarrow$ C7 and C7 $\rightarrow$ C9 (representing the hydrophilic region of IBU), where M_{center} is the center of the ternary micelle. These order parameters were calculated as a function of distance from the center of mass of the ternary micelle, r, and plotted in Figure 9B. For IBU molecules adsorbed on the DPC micelle ($15 < r < 22$), we found $\langle \cos\phi_1 \rangle >> 0$ and $\langle \cos\phi_2 \rangle << 0$, indicating that the hydrophobic portion of IBU faces the core of the micelle and the hydrophilic region away from the micelle. In the region $22 < r < 30$, a secondary shell of IBU forms around the micelle with exactly opposite orientation as those of the first shell (Figure 9B). Thus, in the secondary shell, the hydrophilic region of IBU interacts with the polar head group of the DPC molecules while its hydrophobic methyl groups interact with other IBU and CA molecules in the bulk. Overall, although the hydrophobic effect is the primary driving force for the assembly of these mixed micelles, electrostatic interactions are also important. In other words, the interaction of IBU monomers with DPC on the surface occurs via electrostatic interactions while vdW interactions provide the critical short-range stabilizing force in the core of the ternary micellar complex.

Concluding Remarks

The aim of the present study was to investigate the aggregation behavior of CA and IBU in the presence and absence of a pre-formed PC micelle. To facilitate the formation of micelles/aggregates within reasonable simulation timescales, all-atom explicit solvent molecular dynamics simulations were performed at much higher concentrations than exists at physiological conditions. Based on data from five independent simulations, three for CA:IBU binary mixtures and two for DPC:CA:IBU ternary mixtures, we found that CA and IBU form mixed micelles of various sizes that are in dynamic equilibrium among each other. Aggregation is spontaneous and fast (taking less than 10ns). However, organization after initial assembly takes relatively longer time (10–30ns). The overall morphology of the resulting most populated mixed micelles is similar despite their different sizes. The aggregation behavior of CA and IBU was affected by the presence of a pre-formed DPC micelle. For the same molar ratio, the most populated CA:IBU micelle size was 10 in the presence of DPC compared with 15–19 in its absence. Moreover, though segregated CA and IBU micelles formed on the surface of the DPC micelle, they were small and farther away from each other and thus unable to form larger aggregates. This could be one of the factors behind the reduced-toxicity of PC-conjugated NSAIDs, while the larger mixed micelles in the CA-IBU binary mixtures may be toxic. More broadly, the formation of larger

NSAID:BA micelles with higher NSAID concentrations may explain the relationship between NSAID dosage and toxicity to the lower gut, while PCs may segregate NSAID and BA to prevent the formation of larger and thus potentially more toxic mixed micelles.

Supplementary Material

Refer to Web version on PubMed Central for supplementary material.

References

1. Stix G. A malignant flame. Understanding chronic inflammation, which contributes to heart disease, Alzheimer's and a variety of other ailments, may be a key to unlocking the mysteries of cancer. Sci Am. 2007; 297:8.
2. Singh G, Triadafilopoulos G. Epidemiology of NSAID induced gastrointestinal complications. J Rheumatol Suppl. 1999; 56:18–24. [PubMed: 10225536]
3. Cryer B, Kimmey MB. Gastrointestinal side effects of nonsteroidal anti-inflammatory drugs. Am J Med. 1998; 105:20S–30S. [PubMed: 9715831]
4. Barrios JM, Lichtenberger LM. Role of biliary phosphatidylcholine in bile acid protection and NSAID injury of the ileal mucosa in rats. Gastroenterology. 2000; 118:1179–1186. [PubMed: 10833493]
5. Lichtenberger LM. Where is the evidence that cyclooxygenase inhibition is the primary cause of nonsteroidal anti-inflammatory drug (NSAID)-induced gastrointestinal injury?: Topical injury revisited. Biochem Pharmacol. 2001; 61:631–637. [PubMed: 11266647]
6. Tegeder I, Pfeilschifter J, Geisslinger G. Cyclooxygenase-independent actions of cyclooxygenase inhibitors. FASEB J. 2001; 15:2057–2072. [PubMed: 11641233]
7. Lichtenberger LM. The Hydrophobic Barrier Properties of Gastrointestinal Mucus. Ann Rev Physiol. 1995; 57:565–583. [PubMed: 7778878]
8. Lichtenberger LM, Wang Z-M, Romero JJ, Ulloa C, Perez JC, Giraud M-N, Barreto JC. Non-steroidal anti-inflammatory drugs (NSAIDs) associate with zwitterionic phospholipids: Insight into the mechanism and reversal of NSAID-induced gastrointestinal injury. Nat Med. 1995; 1:154–158. [PubMed: 7585013]
9. Lichtenberger LM, Zhou Y, Dial EJ, Raphael RM. NSAID injury to the gastrointestinal tract: evidence that NSAIDs interact with phospholipids to weaken the hydrophobic surface barrier and induce the formation of unstable pores in membranes. J Pharm Pharmacol. 2006; 58:1421–1428. [PubMed: 17132203]
10. Lanza FL, Marathi UK, Anand BS, Lichtenberger LM. Clinical trial: comparison of ibuprofen-phosphatidylcholine and ibuprofen on the gastrointestinal safety and analgesic efficacy in osteoarthritic patients. Aliment Pharmacol Ther. 2008; 28:431–442. [PubMed: 18549459]
11. Anand BS, Romero JJ, Sanduja SK, Lichtenberger LM. Phospholipid association reduces the gastric mucosal toxicity of aspirin in human subjects. Am J Gastroenterol. 1999; 94:1818–1822. [PubMed: 10406241]
12. Cryer B, Bhatt DL, Lanza FL, Dong J-f, Lichtenberger LM, Marathi UK. Low-Dose Aspirin-Induced Ulceration Is Attenuated by Aspirin-Phosphatidylcholine: A Randomized Clinical Trial. Am J Gastroenterol. 2011; 106:272–277. [PubMed: 21081908]
13. Lichtenberger LM, Barron M, Marathi U. Association of phosphatidylcholine and nsaids as a novel strategy to reduce gastrointestinal toxixity. Drugs Today (Barc.). 2009; 45:877–890. [PubMed: 20135022]
14. Endo H, Hosono K, Inamori M, Nozaki Y, Yoneda K, Fujita K, Takahashi H, Yoneda M, Abe Y, Kirikoshi H, Kobayashi N, Kubota K, Saito S, Ohya T, Hisatomi K, Teratani T, Matsuhashi N, Nakajima A. Characteristics of small bowel injury in symptomatic chronic low-dose aspirin users: the experience of two medical centers in capsule endoscopy. J Gastroenterol. 2009; 44:544–549. [PubMed: 19373431]
15. Fortun PJ, Hawkey CJ. Nonsteroidal antiinflammatory drugs and the small intestine. Curr Opin Gastroenterol. 2007; 23:134–141. [PubMed: 17268241]

16. Goldstein JL, Eisen GM, Lewis B, Gralnek IM, Zlotnick S, Fort JG. Video capsule endoscopy to prospectively assess small bowel injury with celecoxib, naproxen plus omeprazole, and placebo. Clin Gastroenterol Hepatol. 2005; 3:133–141. [PubMed: 15704047]
17. Graham DY, Opekun AR, Willingham FF, Qureshi WA. Visible small-intestinal mucosal injury in chronic NSAID users. Clin Gastroenterol Hepatol. 2005; 3:55–59. [PubMed: 15645405]
18. Yamada T. Mechanisms of acute and chronic intestinal inflammation induced by indomethacin. Inflammation. 1993; 17:641–662. [PubMed: 7906675]
19. Duggan DE. Enterohepatic circulation of indomethacin and its role in intestinal irritation. Biochem Pharmacol. 1975; 24:1749–1754. [PubMed: 823946]
20. Dial EJ, Darling RL, Lichtenberger LM. Importance of biliary excretion of indomethacin in gastrointestinal and hepatic injury. J Gastroenterol Hepatol. 2008; 23:e384–e389. [PubMed: 18086111]
21. Petruzzelli M, Moschetta A, Renooij W, De Smet M, Palasciano G, Portincasa P, Van Erpecum K. Indomethacin Enhances Bile Salt Detergent Activity: Relevance for NSAIDs-Induced Gastrointestinal Mucosal Injury. Dig Dis Sci. 2006; 51:766–774. [PubMed: 16615001]
22. Petruzzelli M, Vacca M, Moschetta A, Cinzia Sasso R, Palasciano G, van Erpecum KJ, Portincasa P. Intestinal mucosal damage caused by non-steroidal anti-inflammatory drugs: Role of bile salts. Clin Biochem. 2007; 40:503–510. [PubMed: 17321514]
23. Venneman NG, Petruzzelli M, van Dijk JE, Verheem A, Akkermans LMA, Kroese ABA, van Erpecum KJ. Indomethacin disrupts the protective effect of phosphatidylcholine against bile salt-induced ileal mucosa injury. Eur J Clin Invest. 2006; 36:105–112. [PubMed: 16436092]
24. Dial EJ, Rooijakkers SHM, Darling RL, Romero JJ, Lichtenberger LM. Role of phosphatidylcholine saturation in preventing bile salt toxicity to gastrointestinal epithelia and membranes. J Gastroenterol Hepatol. 2008; 23:430–436. [PubMed: 17868333]
25. Hofmann AF. The Good, the Bad and the Ugly. News Physiol Sci. 1999; 14:24–29. [PubMed: 11390813]
26. Hofmann AF, Mysels KJ. Bile salts as biological surfactants. Colloid Surface. 1987; 30:145–173.
27. Monte MJ, Marin JJG, Antelo A, Vazquez-Tato J. Bile acids: chemistry, physiology, and pathophysiology. World J Gastroenterol. 2009; 15:804–816. [PubMed: 19230041]
28. Mazer NA, Benedek GB, Carey MC. Quasielastic light-scattering studies of aqueous biliary lipid systems. Mixed micelle formation in bile salt-lecithin solutions. Biochemistry. 1980; 19:601–615. [PubMed: 7356951]
29. Mazer NA, Carey MC, Kwasnick RF, Benedek GB. Quasielastic light scattering studies of aqueous biliary lipid systems. Size, shape, and thermodynamics of bile salt micelles. Biochemistry. 1979; 18:3064–3075. [PubMed: 465453]
30. Ulmius J, Lindblom G, Wennerstrom H, Johansson LB, Fontell K, Soderman O, Arvidson G. Molecular organization in the liquid--crystalline phases of lecithin--sodium cholate-water systems studied by nuclear magnetic resonance. Biochemistry. 1982; 21:1553–1560. [PubMed: 7082635]
31. Boggara MB, Faraone A, Krishnamoorti R. Effect of pH and Ibuprofen on the Phospholipid Bilayer Bending Modulus. J Phys Chem B. 2010; 114:8061–8066. [PubMed: 20518571]
32. Wymore T, Gao XF, Wong TC. Molecular dynamics simulation of the structure and dynamics of a dodecylphosphocholine micelle in aqueous solution. J Mol Struc. 1999; 485–486:195–210.
33. Nelson PH, Rutledge GC, Hatton TA. On the size and shape of self-assembled micelles. J Chem Phys. 1997; 107:10777–10781.
34. Bogusz S, Venable RM, Pastor RW. Molecular Dynamics Simulations of Octyl Glucoside Micelles: Structural Properties. J Phys Chem B. 2000; 104:5462–5470.
35. Lazaridis T, Mallik B, Chen Y. Implicit solvent simulations of DPC micelle formation. J Phys Chem B. 2005; 109:15098–15106. [PubMed: 16852911]
36. Marrink SJ, Tieleman DP, Mark AE. Molecular dynamics simulation of the kinetics of spontaneous micelle formation. J Phys Chem B. 2000; 104:12165–12173.
37. Tieleman DP, van der Spoel D, Berendsen HJC. Molecular dynamics simulations of dodecylphosphocholine micelles at three different aggregate sizes: Micellar structure and chain relaxation. J Phys Chem B. 2000; 104:6380–6388.

38. Partay LB, Jedlovszky P, Sega M. Molecular aggregates in aqueous solutions of bile acid salts. Molecular dynamics simulation study. J Phys Chem B. 2007; 111:9886–9896. [PubMed: 17661512]
39. Verde AV, Frenkel D. Simulation study of micelle formation by bile salts. Soft Matter. 2010; 6:3815–3825.
40. Turner DC, Yin F, Kindt JT, Zhang H. Molecular dynamics simulations of glycholate-oleic acid mixed micelle assembly. Langmuir. 2010; 26:4687–4692. [PubMed: 20112949]
41. Marrink SJ, Mark AE. Molecular dynamics simulations of mixed micelles modeling human bile. Biochemistry. 2002; 41:5375–5382. [PubMed: 11969397]
42. C.D. Warren DB, Hutchison K, Dang W, Pouton CW. Molecular dynamics simulation of spontaneous bile salt aggregation. Colloids Surfaces A. 2006; 280:182–193.
43. Pártay LB, Sega M, Jedlovszky P. Morphology of Bile Salt Micelles as Studied by Computer Simulation Methods. Langmuir. 2007; 23:12322–12328. [PubMed: 17944496]
44. Carey MC, Small DM. Micelle Formation by Bile Salts: Physical-Chemical and Thermodynamic Considerations. Arch Intern Med. 1972; 130:506–527. [PubMed: 4562149]
45. Sayyed-Ahmad A, Lichtenberger LM, Gorfe AA. Structure and Dynamics of Cholic Acid and Dodecylphosphocholine–Cholic Acid Aggregates. Langmuir. 2010; 26:13407–13414. [PubMed: 20695585]
46. Williams K, Day R, Knihinicki R, Duffield A. The stereoselective uptake of ibuprofen enantiomers into adipose tissue. Biochem Pharmacol. 1986; 35:3403–3405. [PubMed: 3768028]
47. Vanommeslaeghe K, Hatcher E, Acharya C, Kundu S, Zhong S, Shim J, Darian E, Guvench O, Lopes P, Vorobyov I, Mackerell AD. CHARMM general force field: A force field for drug-like molecules compatible with the CHARMM all-atom additive biological force fields. J Comput Chem. 2010; 31:671–690. [PubMed: 19575467]
48. Phillips JC, Braun R, Wang W, Gumbart J, Tajkhorshid E, Villa E, Chipot C, Skeel RD, Kalé L, Schulten K. Scalable molecular dynamics with NAMD. J Comput Chem. 2005; 26:1781–1802. [PubMed: 16222654]
49. Darden T, York D, Pedersen L. Particle mesh Ewald: An N.log(N) method for Ewald sums in large systems. J Chem Phys. 1993; 98:10089–10092.
50. Ridell A, Evertsson H, Nilsson S, Sundelöf L-O. Amphiphilic association of ibuprofen and two nonionic cellulose derivatives in aqueous solution. J Pharm Sci. 1999; 88:1175–1181. [PubMed: 10564067]
51. Coello A, Meijide F, Núñez ER, Tato JV. Aggregation behavior of bile salts in aqueous solution. J Pharm Sci. 1996; 85:9–15. [PubMed: 8926591]
52. Coello A, Meijide F, Rodriguez Nunez E, Vazquez Tato J. Aggregation behavior of sodium cholate in aqueous solution. J Phys Chem. 1993; 97:10186–10191.

Highlights

1. Ibuprofen (an NSAID) and Cholic acid (a bile acid) form mixed micelles that are toxic to the intestine.
2. The size of these micelles varies non-linearly with the molar ratio of the reactants.
3. Pre-formed dodecylphosphocholine micelle alters the size of the micelles.

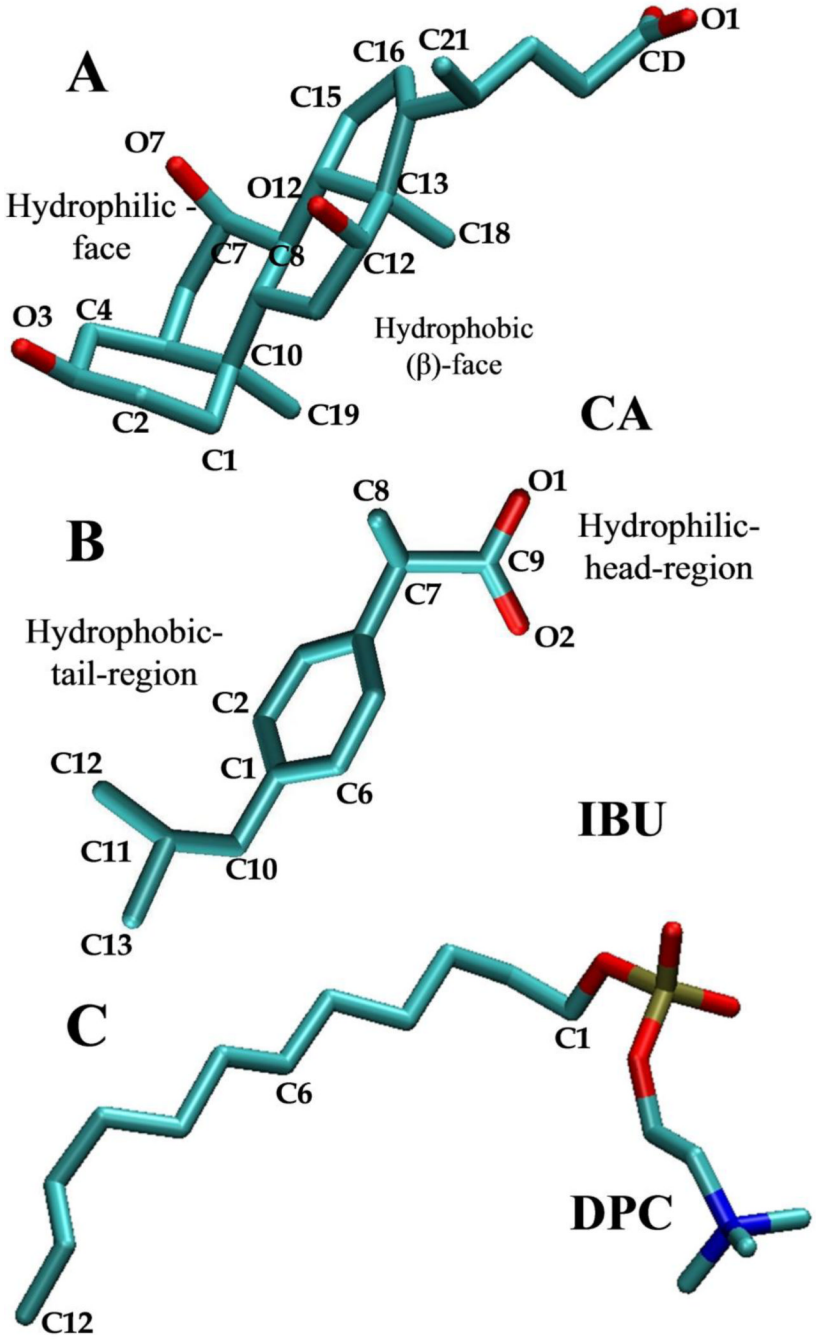

Figure 1.

Chemical structures of **(A)** cholic acid (CA), **(B)** ibuprofen (IBU), and **(C)** dodecylphosphocholine (DPC). Key atoms discussed in the text are labeled. Color code: carbon (cyan), oxygen (red) and nitrogen (blue). Hydrogen atoms are not shown.

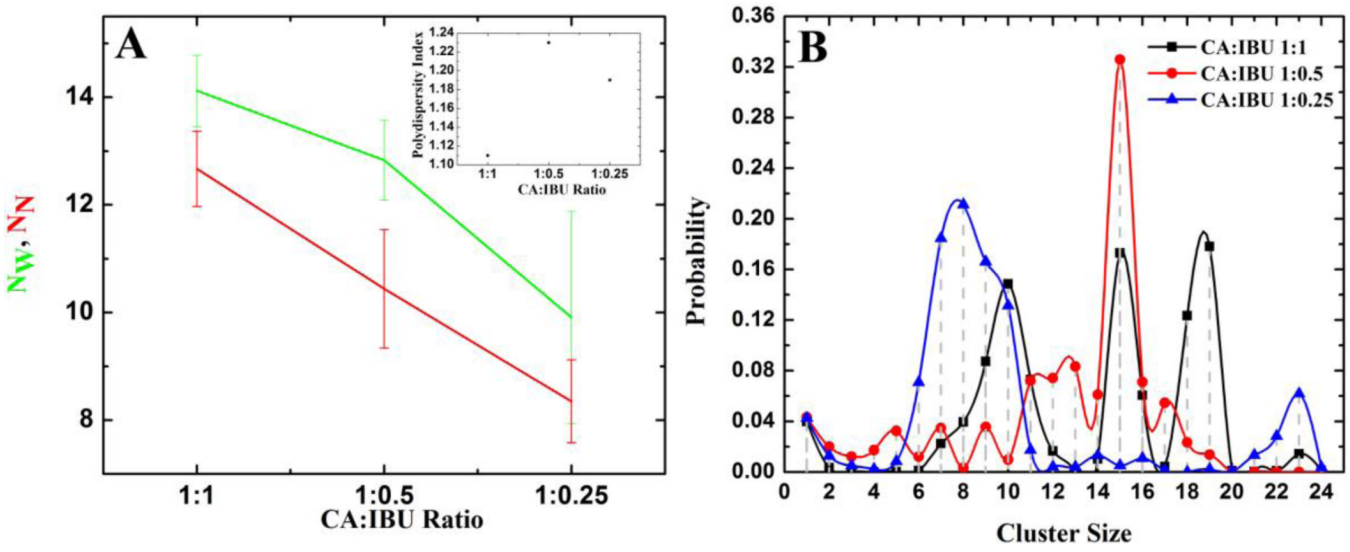

Figure 2.

(A) Ensemble averaged N_W and N_N (main plot) and polydispersity index (inset). **(B)** Weighted probability distribution of the total number of CA and IBU molecules belonging to clusters of size CSn where CSn is defined as the number of CA-IBU mixed micelles of size *n* (*n*=2, 3, 4…) or the number of CA and IBU monomers (*n*=1). For this and subsequent figures the first 30ns of the trajectories was excluded.

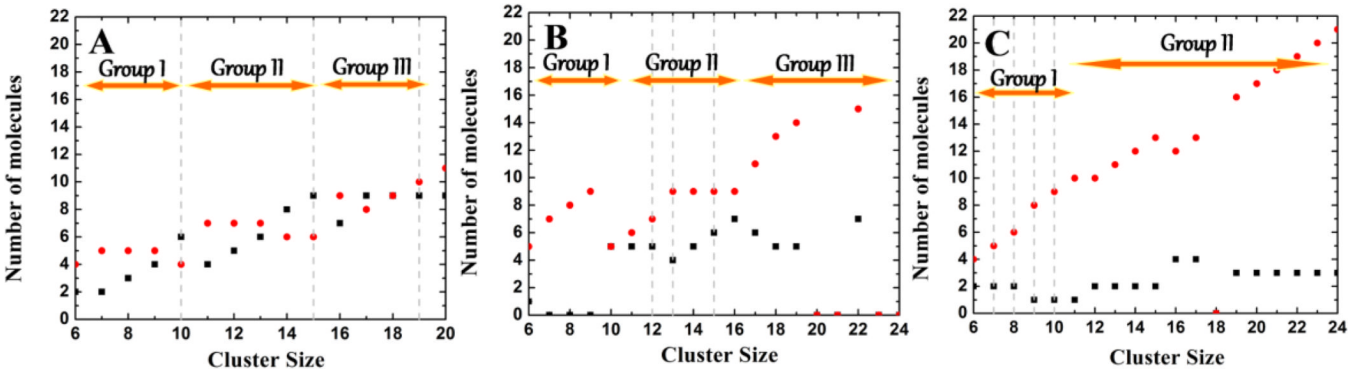

Figure 3.

The average number of IBU (black square) and CA (red circle) molecules belonging to a particular cluster size in simulation S_A **(A)**, S_B **(B)**, and S_C **(C)**. The gray dotted lines represent the most populated micelle sizes shown in Figure 2B.

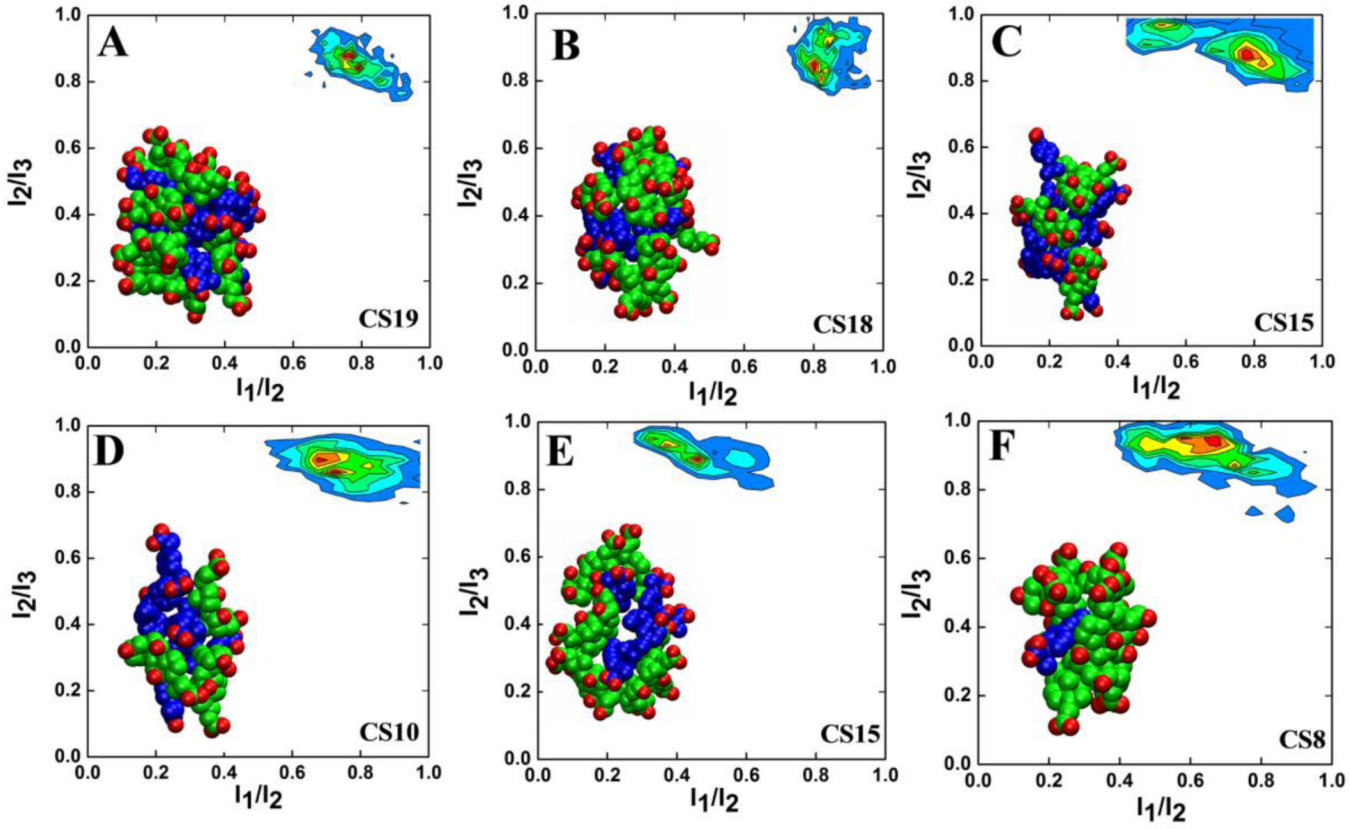

Figure 4.

Bivariate distribution of I_1/I_2 and I_2/I_3 ratios for the predominant micelles from simulation S_A: CS19 **(A)**, CS18 **(B)**, CS15 **(C)**, and CS10 **(D)**; simulation S_B: CS15 **(E)**; and simulation S_C: CS8 **(F)**. Red indicates maximum probability. The principal moments of inertia were calculated from the last 10ns of each trajectory.

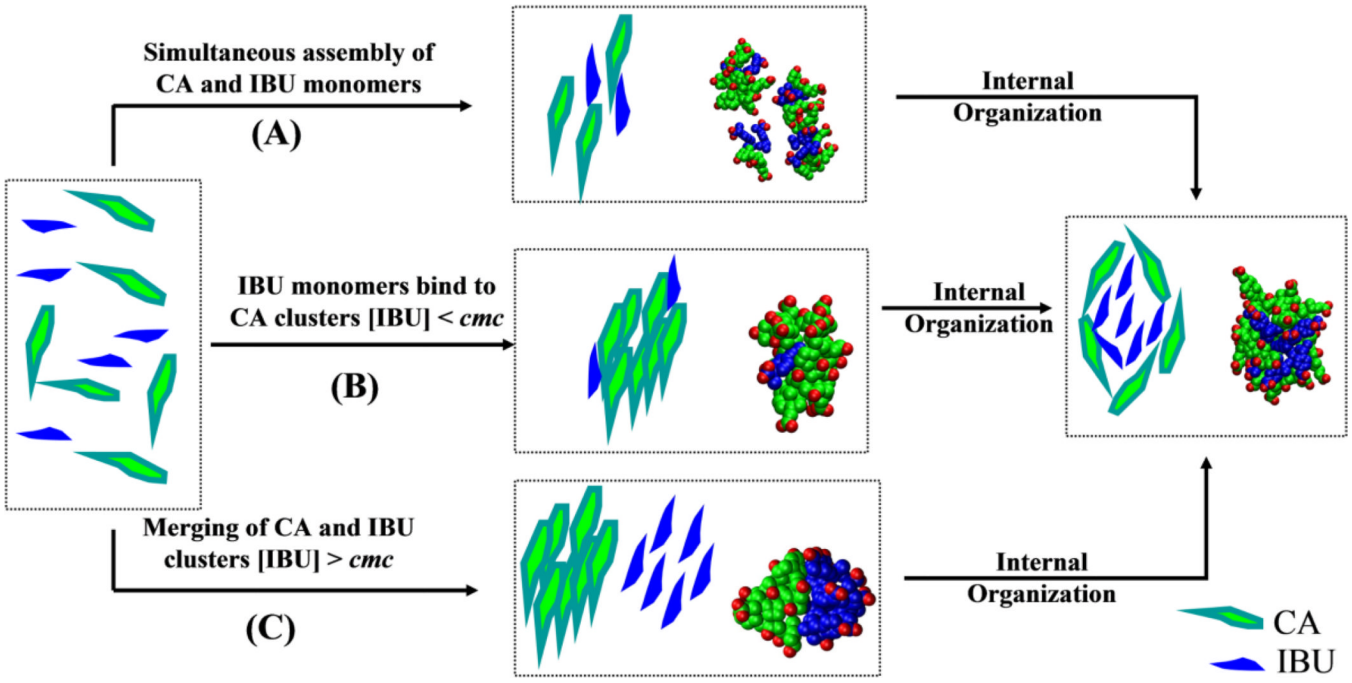

Figure 5.

A proposed mechanism for the aggregation of CA and IBU to form mixed-micelles. CA is shown in green and IBU in blue. Representative snapshots from the simulations are shown for illustration. The information conveyed in this figure is qualitative because limitations in the simulation time scales and the complexity of the process did not allow us to quantify the relative role of each mechanism.

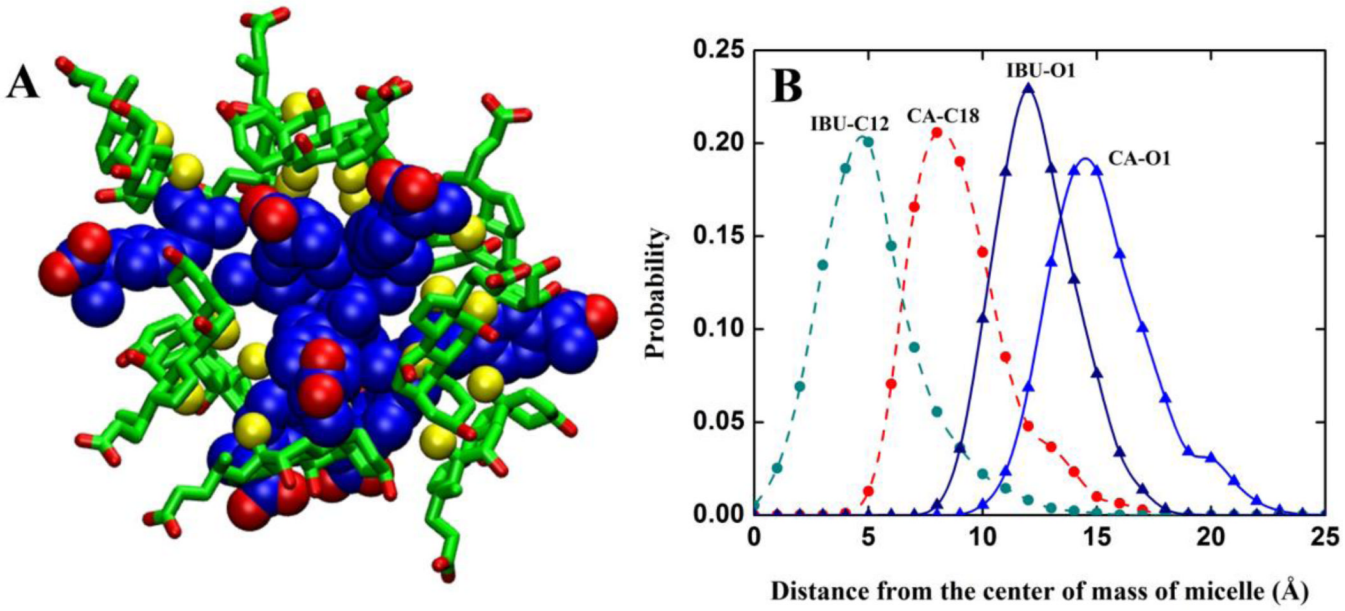

Figure 6.

(A) A 3D representation of the molecular packing in a typical CA:IBU micelle. CA is shown in licorice green with C18 & C19 in yellow spheres. IBU is in blue space-filling model. The oxygen atoms in both CA and IBU are shown in red. **(B)** Average distances between the center of mass and the indicated atoms of micelle CS19 from simulation S_A.

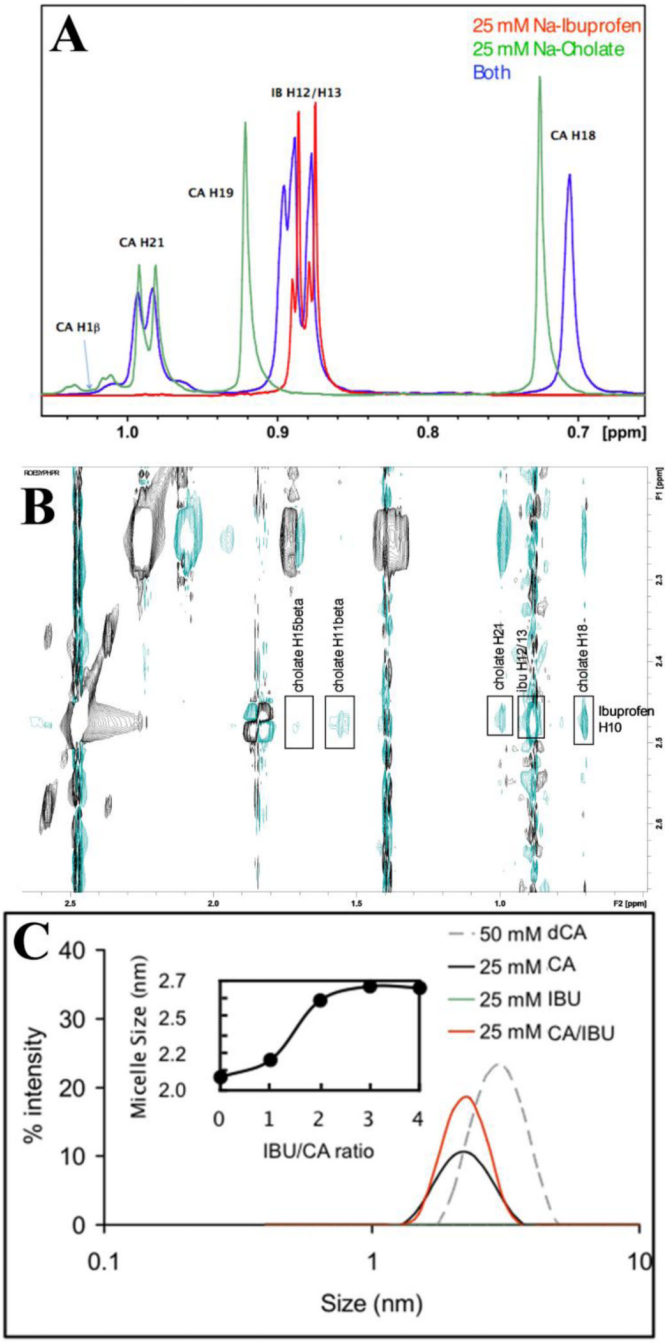

Figure 7.

NMR and DLS characterization of IBU/CA interaction. **(A)** Chemical shifts in a 25mM sample of CA (green), IBU (red) and IBU-CA (blue). **(B)** Portion of a 400 ms ROESY spectrum for a CA-IBU mixture. **(C)** DLS-derived micelle sizes at 25mM for CA (black), IBU (green, which lies on the x-axis) and IBU-CA (red). Micelle size distribution for a 50mM deoxyCA (gray dashed line) is shown for reference. IBU alone did not form micelles at 25mM (green line), and at 5mM had no effect on micelle formation by CA (not shown). Shown in the inset is the average micelle size against IBU/CA ratio, where the sigmoidal

curve indicates increase in micelle size with increasing IBU level until a plateau is reached when IBU is ~3-times more than CA. Refer to Figure 1 for the numbering in (A) and (B).

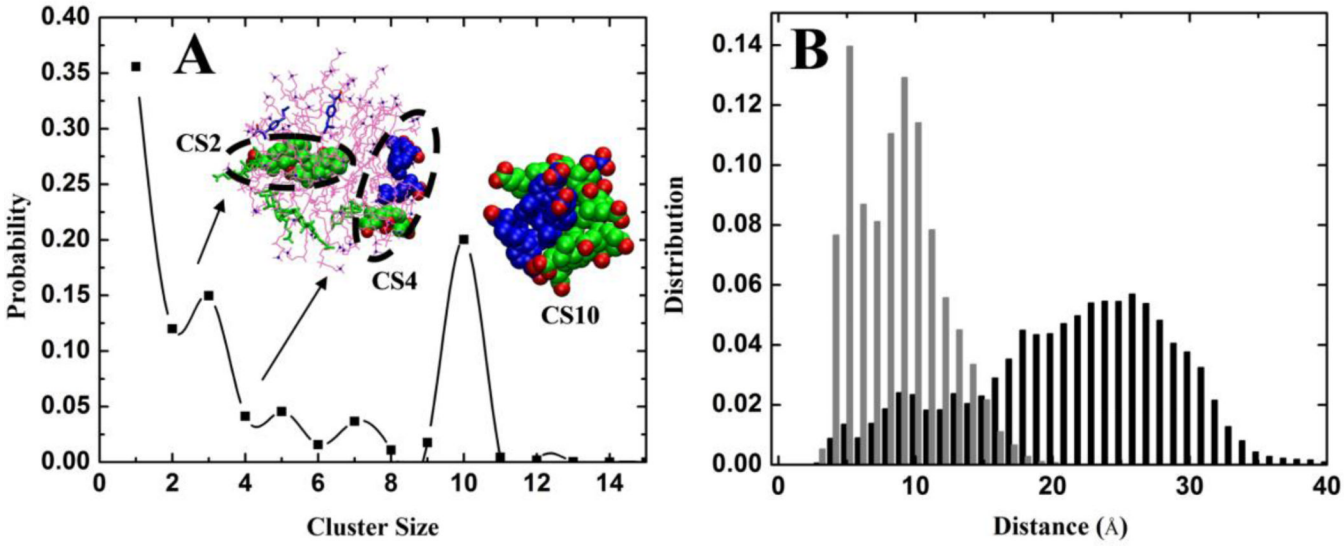

Figure 8.

(A) Weighted probability distributions of the total numbers of CA and IBU molecules belonging to clusters of size CSn from simulation S_E. Two clusters, CS2 and CS4 adsorbed on the DPC micelle, are shown in a space filling model. CA and IBU molecules that are not part of a cluster are shown in licorice. The predominant cluster CS10 found in the aqueous medium is also shown. Very similar results were obtained from S_D (data not shown). **(B)** Distribution of the distances between CA-C18 and IBU-C11 for all CA and IBU molecules in CS10 (gray) and for those within 6Å of the DPC micelle (black). The distribution is calculated for the last 10ns of the simulation. IBU is shown in blue, CA in green and DPC in magenta.

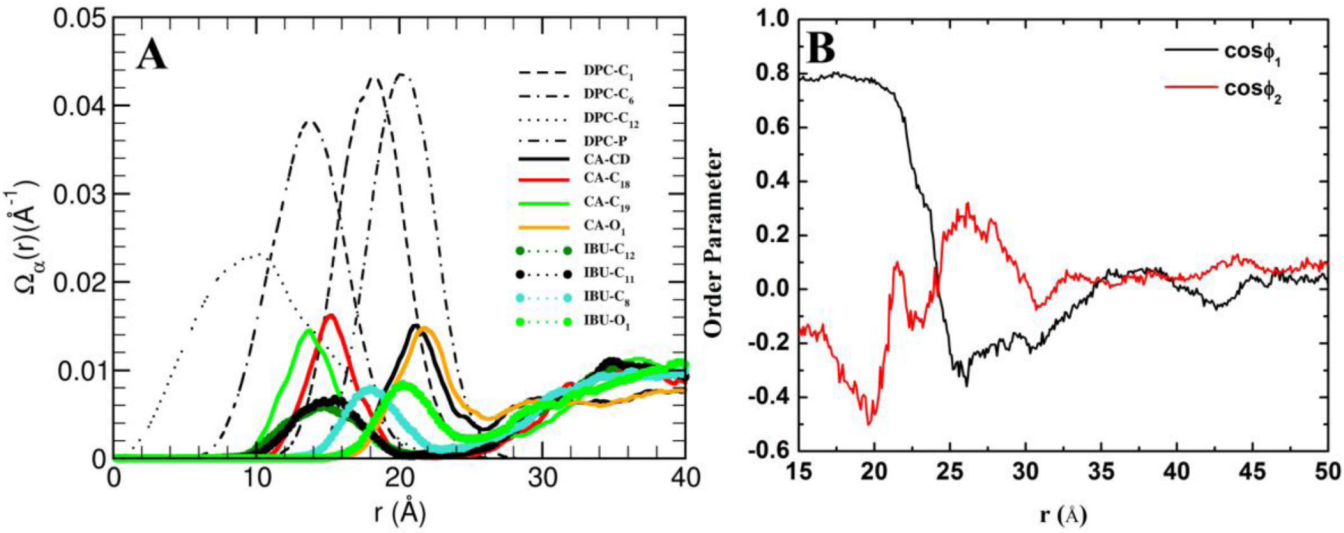

Figure 9.

(A) The distribution of selected atoms as a function of distance from the center of mass of the DPC micelle. **(B)** Orientations of different regions of IBU as a function of distance from the center of mass of the mixed micelle (see text for detail).

Table 1

Summary of the simulations.

Simulation	CA:IBU	DPC-micelle	[CA]mM	[IBU]mM	# of Ions	Simulation Time (ns)
S_A	1:1	-	267 (60) *	267 (60)	120	45
S_B	1:0.5	-	267 (60)	133 (30)	90	60
S_C	1:0.25	-	267 (60)	67 (15)	75	60
S_D	1:1	+ (60)	134 (30)	134 (30)	60	60
S_E	1:1	+ (60)	67 (15)	67 (15)	30	60

* The brackets contain the number of molecules of DPC, CA and IBU. The number of water molecules is 11566 in all cases.

Table 2

Atomic assignments of ROESY cross peaks between IBU and CA.

IBU atom(s)	CA atom(s)
H12/H13	H7
H12/H13	H12
H10	H21
H10	H15a & (H15b or H8b)
H10	H16a & H16b
H10	H2b or H4b or H11b